LBL-26584
UC-402

Lawrence Berkeley Laboratory
UNIVERSITY OF CALIFORNIA

APPLIED SCIENCE DIVISION

RECEIVED
LAWRENCE
BERKELEY LABORATORY
MAY 5 1989
LIBRARY AND
DOCUMENTS SECTION

FY 1988 Annual Report

Environmental Research Program

March 1989

APPLIED SCIENCE
DIVISION

Prepared for the U.S. Department of Energy under Contract Number DE-AC03-76SF00098.

LBL-26584

DISCLAIMER

This document was prepared as an account of work sponsored by the United States Government. While this document is believed to contain correct information, neither the United States Government nor any agency thereof, nor the Regents of the University of California, nor any of their employees, makes any warranty, express or implied, or assumes any legal responsibility for the accuracy, completeness, or usefulness of any information, apparatus, product, or process disclosed, or represents that its use would not infringe privately owned rights. Reference herein to any specific commercial product, process, or service by its trade name, trademark, manufacturer, or otherwise, does not necessarily constitute or imply its endorsement, recommendation, or favoring by the United States Government or any agency thereof, or the Regents of the University of California. The views and opinions of authors expressed herein do not necessarily state or reflect those of the United States Government or any agency thereof or the Regents of the University of California.

LBL-26584

APPLIED SCIENCE DIVISION ANNUAL REPORT

ENVIRONMENTAL RESEARCH PROGRAM

FY 1988

Elton J. Cairns
Director, Applied Science Division

Tihomir Novakov
Program Leader, Environmental Research Program

Applied Science Division
Lawrence Berkeley Laboratory
1 Cyclotron Road
Berkeley, California 94720

Prepared for the U.S. Department of Energy under Contract No. DE-AC03-76SF00098

ENVIRONMENTAL RESEARCH PROGRAM STAFF

Tihomir Novakov, Program Leader
Nancy Brown, Deputy Program Leader

Susan Anderson*
Frank Asaro†
Henry Benner
Charles Blanchard
Nancy Brown†
Shih-Ger Chang†
Robert Cheng
Peck Cho‡
Mariah Cochrane
John Dailey
Raymond Dod
Cheryl Ehorn
Ofodike Ezekoye
David Faris
Luis Feliu
Carlos Fernandez-Pello
Charles Fleischman
Stephanie Frolich
Ian Fry
Robert Giauque
Gloria Gill
Iskander Gokalp*
Philippe Goix
Ralph Greif
Yogesh Gubbi
Lara Gundel
Anthony Hansen
John Harte
Erika Hoffman
Kenneth Hom
Wei-Ming Huang
Gary Hubbard
Margaret Huflejt
Frank Hurlbut
Kristine Ing
Liwen Kao
Arthur Li
David Littlejohn
David Liu
Jau-Huai Lu
Donald Lucas
John Maguire
Julieta Marcelino
Samuel Markowitz
Richard Martin
Andrew Maxson
Rolf Mehlhorn
Harvey Michaels
Helen Michel
Aliza Mizrahi*
Katherine Moore
Fred Mowrer
Amos Newton
Tihomir Novakov†
Bo Ogorevc*
Antoni Oppenheim
Roland Otto
Lester Packer†
Isadore Perlman
Ahmed Rashed
Chang Woo Rhee
Frank Robben
Eva Robinson
Robert Sawyer
Frank Schipperijn
Richard Schmidt
Birger Schmitz*
Richard Schneider
Di-Xiu Shen*
Ian Shepherd§
Linda Sindelar
Gordon Stevens
Horton Stewart§
Fred Stross*
Lawrence Talbot
Louie Tobias*
Eric Wakahiro
Yizhong Wang*
R. Brady Williamson
Linda Wroth
Feng-Hua Yang
Xun Xu

*Participating Guest
†Group Leader
‡University of California Davis
§University of California Berkeley

CONTENTS

Introduction 2-1

ATMOSPHERIC AEROSOLS

Cloud Nucleation Characteristics of Smokes from Different Fuels
A.D.A. Hansen and T. Novakov 2-2

Acceleration of Submicron-Sized Particles
W.H. Benner and R. Otto 2-2

NO_2 and SO_2 Reactions on Cold Surfaces
W.H. Benner, A. Mizrahi, and T. Novakov 2-3

Sulfate Formation by Reaction of SO_2 with NH_3
W.H. Benner, B. Ogorevc, and T. Novakov 2-3

FLUE GAS CHEMISTRY

Removal of NO from Flue Gas by Tetrasulfophthalocyanine Complexes of Iron (II) and Cobalt (II)
D.K. Liu, G. Stevens, and S.G. Chang 2-5

Removal of Nitrogen and Sulfur Oxides from Flue Gas Using Aqueous Emulsions of Yellow Phosphorus and Alkali
D.K. Liu and S.G. Chang 2-5

A Study of the Hydrolysis of Disulfate Ion
D.X. Shen, D. Littlejohn, and S.G. Chang 2-6

The Chemistry of Bisulfite Ion in Aqueous Solution
D. Littlejohn, A. Li, and S.G. Chang 2-6

COMBUSTION

Controlled Combustion
D.W. Faris, K. Hom, J.A. Maxson, A.K. Oppenheim, and H.E. Stewart 2-8

Combustion Chemistry
N.J. Brown and R.J. Martin 2-9

Combustion Fluid Mechanics
R.K. Cheng, I.G. Shepherd, and L. Talbot 2-10

Smoke Emission Measurements from Medium-Scale Experiments
R.B. Williamson, R. Dod, C.M. Fleischman, N. Brown, and T. Novakov 2-11

MEMBRANE BIOENERGETICS

Photochemical Conversion of Solar Energy by Microbial Systems
L. Packer, R.J. Mehlhorn, I.V. Fry, J.J. Maguire, S. Spath, G. Khomutov, W. Nitchmann, E. Hrabeta-Robinson, M. Huflejt, J. Hrabeta, C. Reveron, J. Park, and K. Kondo 2-13

Detection and Prevention of Biological Free Radical Damage
R.J. Mehlhorn, J.J. Maguire, K. Moore, B. Stone, J. O'Neil-Gonzalez, L. Packer, and H. Rapoport 2-14

ANALYTICAL CHEMISTRY

Impacts of Large Extraterrestrial Bodies and Mass Extinctions
F. Asaro, H.V. Michel, L.W. Alvarez, W. Alvarez, and A. Montanari 2-16

A Study of the Relation Between Volcanism in the Weddell Sea about 65 Million Years Ago and the Cretaceous-Tertiary Bolide Impact
H.V. Michael, F. Asaro, W. Alvarez, and and L.W. Alvarez 2-16

Sources of Quartzite in Ancient Egyptian Sculptures
F.H. Stross, R.L. Hay, F. Asaro, H.R. Bowman, and H.V. Michel 2-17

Possible Worldwide Middle Miocene Iridium Anomaly and Its Relation to Periodicity of Impacts and Extinctions
F. Asaro, W. Alvarez, H.V. Michel, L.W. Alvarez, M.H. Anders, A. Montanari, and J.P. Kennett 2-18

ENVIRONMENTAL RESEARCH PROGRAM

INTRODUCTION

The principal objective of the Environmental Research Program is to understand the formation, transformation, transport, and effects of energy-related pollutants on the environment, and how these are influenced by energy generation and emission control technology. Some of the ongoing projects and those that will be initiated in the near future address topics with the general framework of global environmental change. Others deal with studies necessary to understand the fundamentals of generation and effects of environmental contaminants. This multidisciplinary research program includes fundamental and applied research in physics, chemistry, engineering, and biology, as well as research on the development of advanced methods of measurement and analysis. The Program's Annual Report contains summaries of research performed during FY 1988 in the areas of atmospheric aerosols, flue gas chemistry, combustion, membrane bioenergetics, and analytical chemistry.

The main research interests of the Atmospheric Aerosol Research Group concern the chemical and physical processes that occur in haze, clouds, and fogs, and development of novel methods for individual particle characterization.

The Flue Gas Chemistry Research Group is engaged in research whose aim is to help develop new processes for simultaneous SO_2 and NO_x removal.

The Combustion Research Group studies complex combustion processes by acquiring a fundamental understanding of the physical and chemical processes that determine the combustion efficiency, formation, and emissions of species from these processes.

The Membrane Bioenergetics Group studies the effects of strongly chemically reactive compounds generated within cells.

The main emphases in Analytical Chemistry have continued to be in the area of asteroid impacts and mass extinctions.

The short reports that follow describe the program activities in FY 1988. For many of these reports, more detailed papers have been or will be published in appropriate scientific journals.

ATMOSPHERIC AEROSOLS

Cloud Nucleation Characteristics of Smokes from Different Fuels*

A.D.A. Hansen and T. Novakov

Smoke particles from the burning of fuels were historically considered to be hydrophobic; in the more recent past, it was believed that the presence of soluble species (e.g., sulfates) could modify the surface characteristics to make smoke particles more able to act as nuclei for the formation of fog or cloud droplets. However, laboratory measurements of smoke particle incorporation into cloud droplets in condensing plumes had not been widely performed.

In this work, we used our mixing-type cloud chamber to study the behavior of smokes from different fuels and to study the effect of fuel sulfur content on their droplet nucleation characteristics. We burned several liquid fuels (diesel fuel, kerosene, JP-4 jet fuel, Alaskan and Californian crude oils), as well as small fir wood cribs. In some experiments, we added thiophene to the JP-4 to increase its sulfur content. The results showed that the fraction of the mass of smoke incorporated into cloud droplets (under fixed cloud chamber conditions) varied considerably from fuel to fuel, did not bear any relationship to either the fuel sulfur content or the sulfate content of the resultant smoke, and instead depended on combustion efficiency and heat release per unit of fuel consumed. The greater the heat release (progressing, for example, from diesel fuel to jet fuel), the smaller the mass fraction of the smoke incorporated into cloud droplets.

This result suggests that combustion dynamics—and not chemical composition of fuel or smoke—plays a major role in determining water nucleation of smoke particles via their surface characteristics. This result also has implications for assessing the impact of combustion emissions on global climate change.

*This work was supported by the Director, Office of Energy Research, Office of Health and Environmental Research, Physical and Technological Research Division of the U.S. Department of Energy under Contract No. DE-AC03-76SF00098, and by Lawrence Livermore National Laboratory.

Acceleration of Submicron-Sized Particles*

W.H. Benner and R. Otto

We have continued to develop a technique that will eventually be used to determine the elemental composition of individual particles in real time. Three separately constructed components—source of charged particle, a device producing particle beams, and an electrostatic particle accelerator—were coupled and extensively tested as a way to produce particles traveling at ~1 km/sec. In this combined system, NaCl particles having +1 unit of charge and diameters of 0.02, 0.05, or 0.2 μm were generated in the particle source. These particles were then drawn through a differentially pumped skimmer system (particle-beam production), and the resultant beam of particles that traveled at sonic velocity in vacuum served as a way to inject the charged NaCl particles into the electrostatic accelerator. In the electrostatic accelerator, the particles were accelerated through six successively increasing voltage stages with a terminal target voltage of -125 kV. Theoretically, this acceleration produced particles having the velocities 2.4 km/sec, 0.8 km/sec, 0.4 km/sec for particles 0.02 μm, 0.05 μm, and 0.2 μm in diameter, respectively. These stated velocities include a preacceleration velocity of 0.3 km/sec generated by the particle beam system.

After alignment of the components, the system was tested by impacting accelerated particles onto Al and Au targets. Examined by electron microscopy, the targets showed that the impacts produced shallow, smooth-rimmed craters. Some craters contained residue of the impacting particle. These observations indicate that impacts melted most of the NaCl particle but were probably not energetic enough to ionize the particulate material. Our approach for developing a way to ionize particles and determine their composition by mass spectrometry appears feasible, however, because more energetic impacts can be produced by increasing the particle charge and acceleration voltage.

We have begun constructing a particle source that produces test particles of much greater charge. By charging solution droplets as they form and evaporating the solvent, we will produce residual solute particles charged to the Rayleigh limit Theoretically, 0.02-μm, 0.05-μm, or 0.2-μm particles charged to the Rayleigh limit and accelerated through 125 kV will have velocities of 16.8,

*This work was supported by the Director, Office of Energy Research, Office of Health and Environmental Research, Physical and Technological Research Division of the U.S. Department of Energy under Contract No. DE-AC03-76SF00098.

10.7, or 5.2 km/sec, respectively. Particle impacts at these velocities are expected to ionize the particulate components.

NO_2 and SO_2 Reactions on Cold Surfaces*

W.H. Benner, A. Mizrahi, and T. Novakov

Formation of nitrate and sulfate on terrestrial surfaces leads to acidification of the surface because of the accompanying formation of hydrogen ion. The reaction between NO_2^- ion and S(IV) ion in aqueous solution has been studied extensively; much less attention has been paid to reactions on cold surfaces such as ice crystals and frost-covered surfaces.

A chillable glass finger was positioned inside a glass flask that could be charged with several torr of $H_2O(v)$, $NO_2(g)$, $SO_2(g)$ and then filled to atmospheric pressure with clean air. The finger temperature was reduced during several minutes of chilling to produce surface temperatures between room temperature and -45°C. This temperature (reaction temperature) was maintained for 20 min, after which it was rinsed with water. NO_2^-, NO_3^-, S(IV), and $SO_4^=$ were determined in the rinse water by ion chromatography.

The formation of NO_2^- and NO_3^- were observed when the surface was exposed to NO_2 and $H_2O(v)$. The ratio of NO_3^-/NO_2^-, always much greater than 1, was not as expected from the disproportionation of NO_2 in H_2O, where the ratio is 1. The formation of S(IV) and $SO_4^=$ was observed when SO_2 and $H_2O(v)$ were present. When mixtures of NO_2, SO_2, and $H_2O(v)$ were present in the flask, $SO_4^=$ increased and neither NO_2^- nor S(IV) was detected. The general pattern of SO_4^- and NO_3^- formation with respect to reaction temperature was that product increased from a negligible amount at room temperature to a maximum between 10° and -10°C and then decreased to about 50% of the maximum at temperatures below -10°C. The influence of acid catalysis on the product yield was tested by the addition of HCl(g) into the reaction system. Its presence did not appear to change product yield, but maximum sulfate production was shifted to slightly lower temperature.

The reaction between NO_2^- and S(IV) in water primarily produces hydroxylamine disulfonic acid and hydroxylamine monosulfonic acid, but these cannot be hydrolyzed to $SO_4^=$ in the time period of our experiments. Therefore, the observation of $SO_4^=$ formation on the chilled finger suggests that a different reaction occurs, and the oxidation via adsorbed NO_2 is probable. Also, the observed formation of only relatively small amounts of NO_2^- in the absence of SO_2 suggests that the disproportionation of NO_2 in water is affected by physical reaction conditions.

*This work was supported by the Director, Office of Energy Research, Office of Health and Environmental Research, Physical and Technological Research Division of the U.S. Department of Energy under Contract No. DE-AC03-76SF00098.

Sulfate Formation by Reaction of SO_2 with NH_3*

W.H. Benner, B. Ogorevc, and T. Novakov

The absorption of SO_2 into atmospheric droplets provides a reaction medium in which oxidants such as H_2O_2 and O_3, or particle surfaces, can convert SO_2 to $SO_4^=$. The role of NH_3 in this system is that of a buffer and a cation to help maintain ionic charge balance. In the gas phase, SO_2 and NH_3 are known to react to produce many oxy-sulfur products. This gas-phase reaction has been suggested as a source of particulate $SO_4^=$ in the atmosphere but has received little investigative focus. Previous studies examined the types of products formed but not the fractional yield of each product.

A flow system was designed in which 1-100 ppm of each gas in air could be mixed, drawn through a glass reactor, and then bubbled into water. The water vapor content of the gases could also be adjusted from about 1% to 70% relative humidity. After drawing the mixed gases through the system, the reactor was flushed with air and then rinsed with water. The reactor rinse water and the bubbler water were analyzed for $SO_3^=$ and $SO_4^=$ by ion chromatography.

When only SO_2 was drawn through the system, regardless of RH (relative humidity), >95% of the collected sulfur was found in the bubbler; of this percent, >95% was in the form of S(IV). (A small amount of sulfate was found in both the reactor and bubbler.) When equal concentrations (v/v) of SO_2 and NH_3 were drawn through the system, sulfate was observed to form in the reactor but not in the bubbler. Sulfate formation was dependent on the RH, $[SO_2]$, and $[NH_3]$. At 70% RH and 30 ppm of SO_2 and NH_3, as much as 50% of the total SO_2 sampled through the system was oxidized to sulfate. Of the sulfate formed, 95% was always found in the reactor tube. At 30 ppm of each gas and 4% RH, negligible formation of sulfate, when expressed as a percent of the SO_2 drawn through the system, could be attributed to the presence of NH_3. However, when the gas concentrations were reduced to ~1 ppm each, a large percentage of the SO_2 was oxidized to sulfate in the reactor tube.

*This work was supported by the Director, Office of Energy Research, Office of Health and Environmental Research, Physical and Technological Research Division of the U.S. Department of Energy under Contract No. DE-AC03-76SF00098, and by the National Science Foundation under Contract ATM 8713712.

Five findings related to sulfate formation in this reaction system were determined from this work: 1) water vapor is required for the oxidation; 2) the composition of the reactor tube surface influenced sulfate formation — fractional conversion on surfaces increased on the order Teflon < glass < stainless steel; 3) in glass reactors of equal volume, fractional conversion increased as the surface/volume ratio of the reactor tube increased; 4) the

Removal of NO from Flue Gas by Tetrasulfophthalocyanine Complexes of Iron (II) and Cobalt (II)

D.K. Liu, G. Stevens, and S.G. Chang

We have synthesized water-soluble tetrasulfophthalocyanine (TSPc) complexes of iron (III), iron (II), and cobalt (II) according to the procedure of Weber and Busch.[1] The Fe(II)TSPc complex was prepared by using sodium dithionite to reduce Fe(III)TSPc. These metal TSPc complexes have been characterized by elemental analysis as well as by UV-visible and mass spectroscopic techniques. We have demonstrated by UV-visible spectroscopy that the TSPc complexes of Fe(II) and Co(II) can bind nitric oxide to form nitrosyl adducts. Furthermore, we have shown that aqueous solutions of both Fe(II)TSPc and Co(II)TSPc are capable of removing NO from a simulated flue gas mixture containing ~550 ppm NO and variable amounts of O_2 in a wet scrubber system maintained at 55°C. In the case of Co(II)TSPc, the NO absorption reaction was more effective at higher O_2 content. At pH 7, the stoichiometric ratio NO/Co was 0.23, 0.25, and 0.41 at 0%, 5% and 20% O_2, respectively. At pH 3 and 5% O_2, NO/Co was 0.18. Ion chromatographic analyses of the scrubbing liquor showed that ~34% of the absorbed NO was converted to NO_3^-. Purging the scrubbing liquor with O_2 or heating it to ~80°C for 5 h resulted in the recovery of more NO_3^-, with up to ~80% of the NO absorbed accounted for by NO_3^- formation. In the case of Fe(II)TSPc, a NO/Fe ratio of 0.59 was obtained at pH 4.2 with 5% O_2 in the flue gas.

REFERENCES

1. Weber JH, Busch, DH. Complexes derived from strong field ligands. XIX. Magnetic properties of transition metal derivatives of 4,4',4'',4'''-tetrasulfophthalocyanine. *Inorg Chem* 1965; 4:469.

*This work was supported by the Assistant Secretary for Fossil Energy, Office of Coal Utilization Systems, U.S. Department of Energy under Contract No. DE-AC03-76SF00098 through the Pittsburgh Energy Technology Center, Pittsburgh, PA.

Removal of Nitrogen and Sulfur Oxides from Flue Gas Using Aqueous Emulsions of Yellow Phosphorus and Alkali

D.K. Liu and S.G. Chang

We have successfully demonstrated that an aqueous emulsion containing molten yellow phosphorus (P_4; m.p. = 44.1°C) and an alkali such as limestone ($CaCO_3$) can be used for simultaneous removal of NO_x and SO_2 from a simulated flue gas mixture in a wet scrubber. The reaction was carried out at 55°C in a jacketed reactor containing 0.9 *l* of a P_4 (3.3% w/w)/$CaCO_3$ (5.0% w/w) slurry at pH 7.5. The flue gas mixture was composed of 560 ppm NO, 2900 ppm SO_2, 10% O_2, and the balance was N_2. A $CaCO_3$ absorber was placed downstream to capture both P_4- and NO-derived products. As shown in the Figure, ~95% of the NO and all of the SO_2 in the flue gas could be removed for at least 3 h. The solid collected from the scrubber after the reaction was shown by laser Raman spectroscopy to contain $CaSO_4 \cdot 2H_2O$ in addition to

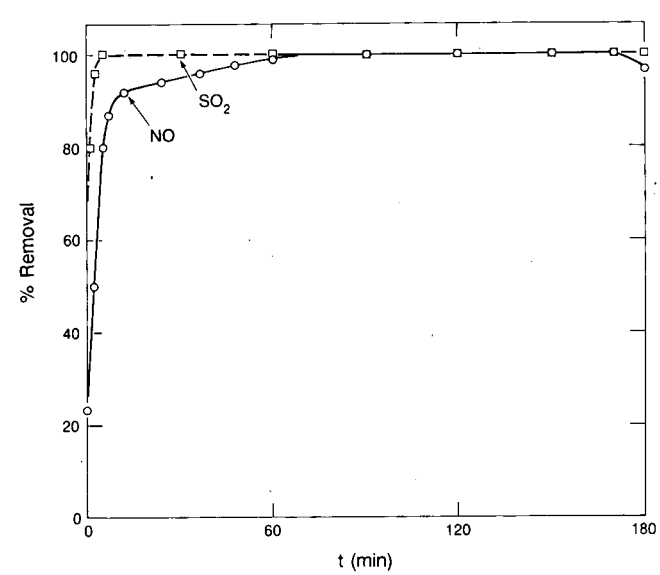

Figure. Simultaneous NO and SO_2 removal from flue gas using a molten yellow phosphorus/limestone slurry. (XBL 886-9664)

*This work was supported by the Assistant Secretary for Fossil Energy, Office of Coal Utilization Systems, U.S. Department of Energy under Contract No. DE-AC03-76SF00098 through the Pittsburgh Energy Technology Center, Pittsburgh, PA.

unreacted $CaCO_3$ and P_4. The liquid phase in both the scrubber and the absorber was analyzed by ion chromatography, revealing the presence of that NO_2^-, NO_3^-, $SO_3^=$, $SO_4^=$, $H_2PO_2^-$, $HPO_3^=$, and $HPO_4^=$. Furthermore, we found that ~40% of the NO absorbed ended up as hydroxylamine disulfonate (HADS) and amine disulfonate (ADS) in scrubbing liquor, both compounds were subsequently hydrolyzed to NH_4^+. Therefore, the use of yellow phosphorus and an alkali for combined NO_x and SO_2 removal could result in production of valuable fertilizer materials, including ammonium nitrate and phosphate.

A Study of the Hydrolysis of Disulfate Ion

Di-Xen Shen, David Littlejohn, and Shih-Ger Chang

In an earlier study of the oxidation of bisulfite ion, we discovered that the oxidation reaction proceeds via an intermediate, determined to be disulfate ion, which then hydrolyzes to form sulfate ions and hydrogen ions. Other researchers had found that the rate of hydrolysis was influenced by other ions in solution. We have systematically investigated the effect of ions found in scrubbing solutions on the hydrolysis of disulfate ion.

The disulfate salt was mixed with a solution of the ion under study, and the reaction was monitored by two techniques. Raman spectrometry permitted observation of the decay of the disulfate ion and the growth of sulfate and bisulfate ions. However, the low concentrations often used in the study yielded weak signals, making accurate determination of the rate difficult. Use of a recording pH meter with a fast-response pH probe to record the change in pH of the solution proved to be simpler and more accurate than Raman spectrometry. This method was used for most measurements.

A number of cations and anions have been studied. Magnesium and calcium ions, often found in scrubbing solutions, greatly increased the hydrolysis rate. Of the anions studied, sulfite and thiosulfate were found to produce the largest hydrolysis rate increases. The results are shown in the Figure, where the observed rate constant for disulfate hydrolysis at 20°C is displayed for the ions studied. We are currently studying the influence of other ions on disulfate ion hydrolysis. These results will allow calculation of the lifetime of disulfate ion in scrubbing solutions.

*This work was supported by the Assistant Secretary for Fossil Energy, Office of Coal Utilization Systems, U.S. Department of Energy under Contract No. DE-AC03-76SF00098 through the Pittsburgh Energy Technology Center, Pittsburgh, PA.

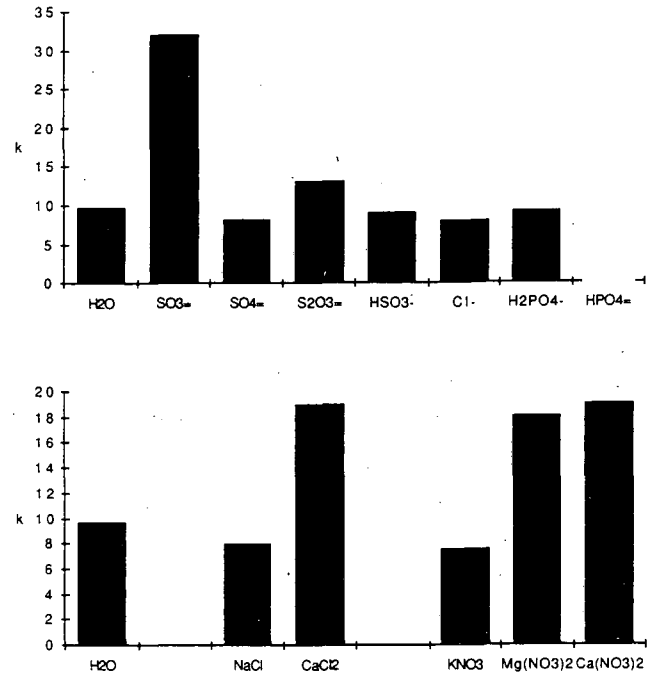

Figure. Effect of cations (upper) and anions (lower) on disulfate ion hydrolysis. (XBL 8811-3937)

The Chemistry of Bisulfite Ion in Aqueous Solution

D. Littlejohn, A. Li, and S.G. Chang

Bisulfite ion is the dominant form of SO_2 dissolved in aqueous solutions over a pH range of 2 to 7. Flue gas cleanup processes using aqueous solutions to remove SO_2 often have high concentrations of bisulfite ion. To properly treat these scrubbing solutions, the chemistry of bisulfite ion must be understood; however, it is fairly complicated. Bisulfite can exist in two isomeric forms and can form one- and possibly two- dimers. Using NMR, Horner and Connick[1] obtained a measure of the bisulfite isomerization equilibrium constant. They assigned NMR peaks to the isomers indirectly.

We have used Raman spectroscopy to observe the effect of temperature on low-concentration solutions of bisulfite ion. Spectra of solutions with pHs of 2.1, 4.2, and 6.6 were obtained at three temperatures: 278K, 298K,

*This work was supported by the Assistant Secretary for Fossil Energy, Office of Coal Utilization Systems, U.S. Department of Energy under Contract No. DE-AC03-76SF00098 through the Pittsburgh Energy Technology Center, Pittsburgh, PA.

and 333K. The solutions had a concentration of 0.1M in total S(IV). From the temperature dependence of the peaks in the spectra, we were able to assign two previously unassigned Raman peaks. The 1023 cm^{-1} Raman band is from the $HOSO_2^-$ bisulfite isomer; the 1052 cm^{-1} band is from the HSO_3^- isomer.

The relative intensities of the bands were used to determine the equilibrium constant for the isomers. Because the strength of the Raman bands cannot be easily predicted, the 298K equilibrium constant value of Horner and Connick[1] was used to determine the intensity ratio of the 1023 cm^{-1} and 1052 cm^{-1} bands. With this information, we calculated the equilibrium constant as a function of temperature (Figure). No significant difference was observed between the three pH conditions. From the sum of the results, we obtain an expression for the equilibrium constant:

$$\ln K = (-1.91 \pm 0.23) + (1032 \pm 70)/T$$

where $K = (HOSO_2^-) / (HSO_3^-)$. From this expression, values of $H = -2.1 \pm 0.2$ kcal mol^{-1} and $S = -4 \pm 0.5$ cal K^{-1} mol^{-1} are derived. Much more work must to be done on the chemistry of this system, including that associated with the dimer or dimers.

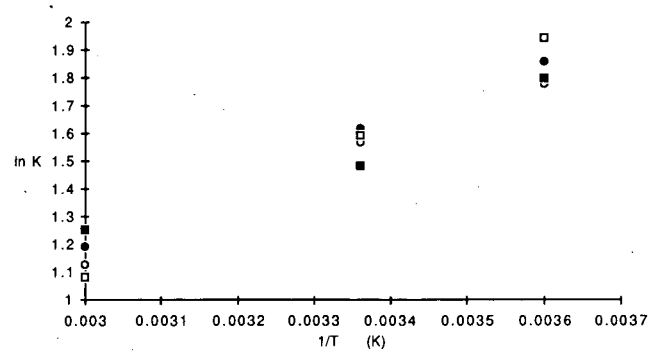

Figure. Plot of the log of $(HOSO_2^-)/(HSO_3^-)$ vs 1/T. Key: solid circle - pH 2.1, open circle - pH 4.2, solid square - pH 6.6, open square - values of Horner and Connick. (XBL 8811-3938)

REFERENCES

1. Horner DA, Connick RE. Equilibrium Quotient for the Isomerization of bisulfite ion from HSO_3^- to SO_3H^-. *Inorg Chem* 1986; 25:2414.

COMBUSTION

Controlled Combustion*

D.W. Faris, K. Hom, J.A. Maxson, A.K. Oppenheim, and H.E. Stewart

The major purpose of this study is to provide a scientific basis for developing controlled-combustion engines. Pragmatically, such engines have the prospect of minimizing the formation of pollutants, optimizing the tolerance to a wide assortment of fuels, and maximizing fuel economy. In order to attain such a goal, combustion chambers-considered so far as just sources of motive power-have to be converted into fully controllable chemical reactors. In principle, this involves a fundamental modification of the process of combustion in that, instead of having to rely on the Flame Traversing the Charge (FTC) system used universally today, combustion is carried out within regions of well-stirred reaction zones. This mode of combustion can be accomplished by a Pulsed Jet Plume (PJP), a turbulent plume formed by a pulsed jet generated by combustion in a cavity of an igniter plug of C type described previously.† Our studies became focused on exploring the prominent features of jet ignition and the dynamic effects of the exothermic process of combustion taking place within a predesignated elementary region of the reactor (the head space in an engine).

Further studies using our numerical modeling techniques and evaluation of fluid mechanics of flames propagating in enclosures[1-3] presented a basis for identifying the essential aspects of a controlled-combustion engine.[4] We also completed experimental tests of pulsed plasma jet igniters[5] and the computational investigations of the dynamic effects of exothermic combustion centers.[6]

Using our molecular beam mass spectrometer, we succeeded in measuring 1) species concentration histories in the plume of a pulsed plasma jet igniter during ignition and 2) subsequent combustion of methane/oxygen, nitrogen and methane/oxygen/argon mixtures. Equivalence ratios of 1.0, 0.6, and 0.4 were used in the igniter cavity and in the main combustion chamber to provide both combusting and non-combusting cases. Species measurements indicate that combustion initiated by plasma jets can be divided into three phases. The hot initial stage is dominated by high-temperature species formed in the plasma cavity and in the turbulent plume, entrainment continues in a second region, with generation of products in the plume but not in the bulk gas mixture. High radical concentrations characterize the first stage; N atoms peak at a mole fraction of 0.004, and OH reaches a value of 0.007 in the stoichiometric case. The second stage involves the reactions of intermediate products such H_2, NO, and CO along with the production of final, stable products. In the final stage, CO_2 and H_2O concentrations rise to levels expected from complete combustion of the reactants. These measurements are used to explain how pulsed plasma jets enhance ignition in lean mixtures.

We computed the dynamic effects of a local exothermic center for a number of representative gaseous fuel/air mixtures in cases where reliable chemical kinetic models are available. Fuels under consideration included hydrogen, methane, acetylene, ethylene, and ethane. This study was based on the premise that exothermic centers arise from inhomogeneities in the bulk mixture and ignite earlier than the surrounding mixture. The model of an exothermic center considers thus a small, homogeneous mass of reacting mixture surrounded by an essentially inert mixture. In the analysis, the energy and species equations for the reacting mixture are combined with the gas dynamic constraints for expansion of the exothermic kernel in the center. Induction time, excitation time (rise time of the exothermic power pulse), and exothermic energy and power of the centers are then evaluated. An important dynamic effect of the center is the compression wave it produces in the surrounding mixture. Computations show that compression ratios of 1.2 to 1.8 are achieved at elevated initial pressures in the exothermic centers we studied.

With this as a background, we turned our attention to the physics and chemistry of combustion in PJP's. Preliminary experiments were run in a constant-volume, cylindrical vessel, providing an unobstructed optical insight along the axis for schlieren photography. The progress of the exothermic process was monitored by pressure transducer records. The results demonstrated the superiority of this mode of combustion as compared with the FTC system tested under identical operating conditions and revealed the ability of a PJP to entrain (inhale) the surrounding mixture into its midst for chemical processing inside the region of space it occupies, being spread across the surroundings by a propagating (self-advancing) flame front. Further exploration of the characteristic features of combustion by PJP's have thus become the principal goal of our project.

To study the physical and chemical processes taking place in an exothermic PJP, experimental investigations will use a constant-volume vessel used for preliminary experiments and a shock tube to test the operating features of PJP's under high initial pressures and temperatures (as well as turbulence level) and resembling those of internal combustion engines.

*This work was supported by the Director, Office of Energy Research, Office of Basic Energy Sciences, Engineering and Geosciences Division, of the U.S. Department of Energy under Contract No. DE-AC03-76SF00098, and by the U.S. Army Research Office under Contract No. DAAL03-87-K-0123.

†*Applied Science Division FY87 Annual Report*, p. 2-17 (Fig. 2), March 1988. (LBL-24212)

Associated with this, we will conduct an analytical effort to explore the mechanism of the flow field generated by a PJP, based on numerical modeling techniques we are currently adopting for this purpose.

REFERENCES

1. Rotman DA, Oppenheim AK. Aerothermodynamic properties of stretched flames in enclosures. *In: Twenty-First Symposium (International) on Combustion.* The Combustion Institute, 1986; 1303-1312.
2. Giovannini A, Oppenheim AK. Analyse de different types d'ecoulements internes par la methode des vortex aleatoires. *J Theoret App Mech,* 1987; *6*: 771-787.
3. Chau EL, Rotman DA, Schipperijn FW, Oppenheim AK, Sawyer RF, Iiyama A, Xia, LQ. Experimental and Numerical Modeling Study of Engine Combustion. SAE Paper 872103, 1987.
4. Oppenheim AK. Quest for Controlled Combustion Engines. SAE Paper 880572, 1988.
5. Lucas D, Cavolowsky JA, Breber PR, Oppenheim AK. Pulsed Plasma Jet Igniters: Species Measurements in Methane Combustion. Presentation at the 22nd International Symposium on Combustion, University of Washington, Seattle, WA, August 1988.
6. Lutz AE, Kee RJ, Miller, JA, Dwyer HA, Oppenheim AK. Dynamic Effects of Autoignition Centers for Hydrogen and $C_{1,2}$-Hydrocarbon Fuel. Presentation at the 22nd International Symposium on Combustion, University of Washington, Seattle, WA, August 1988.

Combustion Chemistry*

N.J. Brown and R.J. Martin

Chemical reactivity, energy transfer, transport processes, and fluid mechanics govern combustion processes. Our research is primarily concerned with understanding the first two of these so that better control over combustion can ultimately be achieved. Advances of theories of reactivity have important impacts on our understanding of the chemistry affecting the emissions of pollutant species, rates of heat release during combustion, and the growth rates of undesirable combustion phenomena.

Research continued on the use of functional sensitivity analysis[1] to measure the response of dynamical observables to arbitrary variations of the potential energy surface at given points in configuration space. This research is being conducted in collaboration with Herschel Rabitz and Richard Judson of Princeton University. Particular attention was given to representing the complete sensitivity functions for the two dimensional/two molecule/rigid rotator problem. In Figure 1, radial slices of these are shown for the HD molecule. Each panel shows the function for a fixed value of R, the separation between the center-of-mass for each molecule given in bohr. The abscissa is the polar angle of molecule 1 (H_2), while the ordinate is the angular coordinate for molecule 2 (HD). Solid contours indicate positive values; dotted contours indicate negative values. These contours provide direct evidence of molecule/molecule behavior.

Studies of rotational relaxation in the HD + HD system were completed, and energy transfer rates from more initial states were determined. Agreement between

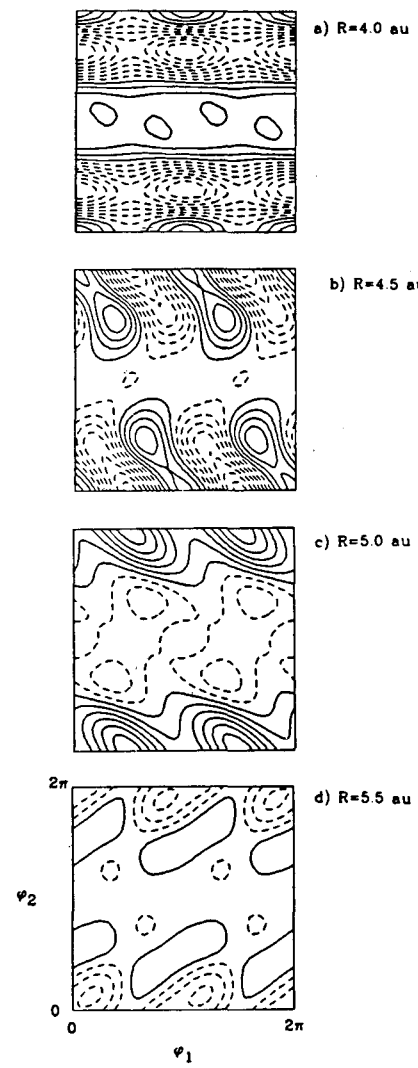

Figure 1. Radial slices of the full log-normalized sensitivity function for the change in rotational energy in HD. The ordinate and abscissa are given in polar angles for fixed values of the radial coordinate. (XBL 891-92)

*This work was supported by the Director, Office of Energy Research, Office of Basic Energy Sciences, Chemical Sciences Division of the U.S. Department of Energy under Contract No. DE-AC03-76SF00098.

theoretical and experimental rotational energy transfer rates was within an order of magnitude and was considerably better for transitions to neighboring states.

We performed a complete Monte Carlo calculation of the H_2 + OH rate coefficient for the temperature range 750 to 4000 K, and agreement with experimentally determined and transition state values was very satisfactory. Energy rejection techniques were used in this calculation, and these corrected for zero-point problems encountered in conventional quasi-classical approaches.

A review paper is being written on rate coefficient calculations for combustion modeling studies. Major topics in the review are potential energy surfaces, various forms of transition state theory, quasi-classical dynamics, and sensitivity analysis.

Research also continued[2] on the modeling of N_2O combustion chemistry; these calculations were performed in concert with sensitivity calculations. We are modeling premixed laminar flames where N_2O is formed and destroyed, and we have achieved excellent agreement between calculations and experiments.

We plan to pursue research on the functional sensitivity analysis as a tool for probing the mechanisms of molecular collisions. In addition, we expect to complete our review paper on rate coefficient calculations for combustion modeling studies. Modeling of our laminar flame experiments and flash-ignited combustion experiment will also be completed.

REFERENCES

1. Judson RS, Rabitz H, Brown NJ. A classical functional sensitivity analysis of coplanar inelastic scattering for H_2 + H_2 and its isotopic analogs. (*J Phys Chem*, in press, 1988)
2. Martin RJ, Brown NJ. The importance of thermodynamics to the modeling of nitrogen combustion chemistry. (*Combustion and Flame*, in press, 1988)

Combustion Fluid Mechanics*

R.K. Cheng, I.G. Shepherd, and L. Talbot

Turbulent combustion is the dominant mode of operation in most engines and burners because fluid mechanical turbulence enhances the burning rate. The coupling between turbulence and combustion chemistry is very complex, and the interactions involve significant temperature, velocity and pressure fluctuations in both space and time. Fluctuations affect reaction rate as well as concentrations in the combustion exhaust. Moreover, because the range of chemical and fluctuation time scales span many orders of magnitude, experimental studies and the development of turbulent combustion theory present major challenges to combustion scientists today.

One of the most viable means of gaining a better physical understanding of the controlling turbulence-combustion interaction processes is by investigating the combustion flowfields in laboratory scale burners. These experiments are designed so that the fluid mechanical time scales are large compared to the chemical time scales so that theoretical treatment of the combustion chemistry can be simplified. By use of laser diagnostic techniques which measure scalar and velocity fluctuations and other statistical cross-correlations, data are obtained for comparing and evaluating current theoretical models and for determining the effects of turbulence intensity on burning rates.

For premixed turbulent combustion studies where the fuel and the oxidizer are thoroughly mixed prior to combustion, we use three laboratory burners of different geometries: rod-stabilized "v" flames, large conical Bunsen type tube-stabilized flames, and planar flames stabilized in the stagnation flow. The burners are designed to provide the best possible data for comparison with current one-dimensional (1-D) or two-dimensional (2-D) theoretical models. One of our significant recent achievements is the development of an experimental procedure to trace the flow path through the flame zone. This procedure is based on automatic feedback control of a two-component laser Doppler anemometry (LDA) system which measures in-situ flow velocities. Examples of flowpaths determined within a methane/air v-flame are shown in Fig. 1. The flowpaths are clearly not aligned with the principal axes of the burner; therefore, previous measurements made along fixed vertical or horizontal axes may have led to erroneous conclusions. The physical significance of the flowpaths is also confirmed by the development of a novel method for determining overall burning rate, based on reaction-rate data obtained along these paths.

The statistics on velocity along the flowpaths also show the influence of burner geometry. This is due to flow acceleration induced by combustion heat release which modifies the characteristic pressure field of burners with different geometric contraints. Consequently, the turbulence intensity in the burned region depends on whether the pressure increases (as in the stagnation flow region) or decreases (as in the v-flames) downstream from the flame. Modeling of the evolution of the turbulence intensity within the flame zone requires empirical data. Because reliable diagnostic methods for measuring pressure fluctuations are not available, the velocity data remain the only means of inferring changes in the pressure field. We plan to continue our analysis of the velocity data along the flow paths. In particular, the magnitudes of the flow acceleration and changes in turbulence intensities will be compared for various flames with different turbulence and fuel/air ratios.

Another aspect of the flame-flow interaction which has not been explored in detail is the effect of the flame on the non-reacting region upstream of the reaction zone.

*This work was supported by the Director, Office of Energy Research, Office of Basic Energy Sciences, Chemical Sciences Division of the U.S. Department of Energy under Contract No. DE-AC03-76SF00098.

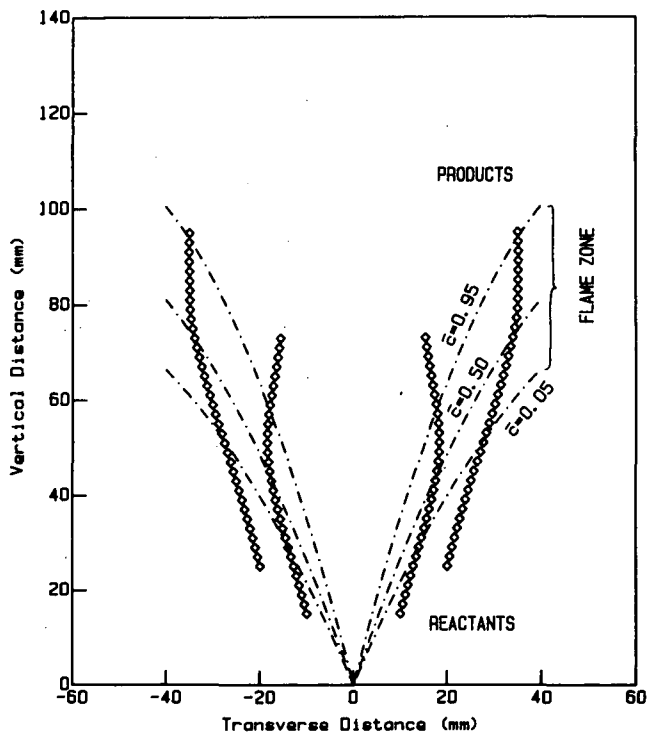

Figure Example of flowpaths through a methane/air v-flame as determined by automatic feed-back control of a 2 component Laser Doppler anemometry system. flow path positions. (XBL 8811-3853)

The velocity time scales deduced by spectral analysis show some changes. Comparison of the velocity time scales with the time scales of the temperature fluctuations within the reaction zone have provided some evidence that the two scales are related. Because the time scales of the temperature fluctuations are associated with reaction rate, such comparison will be useful for quantifying the relationship between turbulence intensity and burning rate. As most current models do not consider the effects of combustion in the upstream region, our investigation is expected to show whether or not these effects warrant theoretical treatment.

In FY88, we initiated two experiments for studying turbulent non-premixed (diffusion) flames. In non-premixed flames, mixing of the fuel and the oxidizer occur simultaneously with combustion. The flowfields are more complex than those of the premixed flames. The two experiments both use a fuel jet issuing into co-flow or opposed flow of air. The flow and mixture conditions are designed so that the turbulence time scales are large compared with the chemical times. Using various flow visualization techniques, we have thus far obtained preliminary data on the shape of the reaction zone. Measurement of the velocity statistics are well underway and will be continued.

In addition to our experimental efforts, progress has also been made in our numerical study of premixed turbulent flames using the vortex dynamic technique. The numerical work complements the experimental studies. We have explored means of improving the algorithm for describing the flame movements. The flame movement within the reaction zone consists of two components. The first is associated with the transport of the flame by the mean flow; the second is caused by flame propagation. Because flame propagation represents the fuel consumption rate, it is directly related to the turbulent burning rate. Previous algorithms assume that the flame propagates everywhere at a constant burning speed. This technique cannot consider the effects of flame curvature or the effects of flame cusps. A new flame movement algorithm developed by Prof. J. Sethian for vortex dynamic simulations of premixed turbulent flames is capable of overcoming these limitations, and this algorithm is being incorporated into our numerical program for the v-flames. The evolution of the shape of the flame interface predicted by this model will be compared with those obtained experimentally by tomography. Also deduced from the numerical results are the conditioned velocity statistics, which can be compared with previously obtained experimental data.

Smoke Emission Measurements from Medium Scale Experiments*

R.B. Williamson, R. Dod, C.M. Fleischmann, N.J. Brown, and T. Novakov

The concept of a "nuclear winter" has been postulated with a number of assumptions regarding the smoke produced by post-nuclear exchange fires. Knowledge of the quantity and character of the smoke emitted by those fires is crucial for predicting their climatic impact.

To help quantify the smoke which might be generated after use of nuclear weapons - and which may cause a "nuclear winter" - we conducted a series of medium-scale fire experiments using representative urban fuels such as wood, asphalt roofing, and liquid petroleum.

More than 20 medium-scale experiments were conducted in this research program. During each experiment, the mass smoke was determined by sampling the aerosol particulates in the exhaust duct which captured the effluent from the burning material, and the rate of heat release (RHR) was measured by oxygen depletion calorimetry (ODC). In addition, the characteristics of the smoke, and particularly its graphitic ("black") carbon content, were analyzed. Another important, unique aspect of this research is that some experiments were conducted with limited ventilation by burning materials in a compartment having only a window to admit air inside.

*This work was supported by the Defense Nuclear Agency through the U.S. Department of Energy under Contract No. DE-AC03-76SF00098.

The smoke emission factors measured for burning wood under well-ventilated conditions ranged from 0.1% to 0.3%, but under limited conditions this increased an order of magnitude, i.e., to between 1% and 3%.

For No. 2 fuel oil, the well-ventilated smoke emission factor ranged from 8% to 10%, but when the oil was burned in the compartment, the emission factor dropped to 5%. This experiment was not "ventilation limited"; approximately twice as much oxygen was present than would have been necessary for burning all the fuel volatilized per unit time. This decrease in emission factor for the oil burned in the compartment is probably attributable to the higher temperature resulting from radiative feedback in the compartment (as compared with the open pan fire) and to more complete combustion resulting in substantial soot burnout.

The smoke emission factors measured for asphalt under well-ventilated conditions were approximately 12%. Asphalt was not burned in the compartment.

In the context of a "nuclear winter," the implications of these measurements are centered around four concepts. First, ventilation has a substantial effect on smoke production from burning wood and oil; the emission factors for wood measured under limited ventilation conditions were more than an order of magnitude higher than those measured under well-ventilated conditions. More importantly, the smoke in the compartment fire was thick and black, similar in appearance to the smoke produced by burning plastic or oil. Wood is one of the major building and furnishing materials used in the United States, and we may reasonably assume that large quantities of wood would burn under both limited and unlimited ventilation conditions in the post-nuclear environment.

Second, the well-ventilated medium-scale wood experiments produced several orders of magnitude more black carbon than did previously reported bench-scale experiments. The black carbon particles absorb sunlight and produce the "nuclear winter" effects.

Third, the smoke emission factors for asphalt roofing shingles (a total of more than 12% with 90% being black carbon) could have a significant impact on urban smoke production in the post-nuclear environment.

Fourth, our experimental results to date show an important trend: the smoke emission factors for oil decrease as fire size or intensity is increased. The smoke emission factors were more than 10% for the single-pan experiments but decreased when the fire was doubled or placed in the compartment.

For FY 89, we plan to continue the medium-scale experiments with increasing rates of heat release under various ventilation conditions in order to evaluate the effects of scaling. In particular, we will emphasize the study of scaling between our experiments and will explore ways of correlating our findings with those of other investigators.

MEMBRANE BIOENERGETICS

Photochemical Conversion of Solar Energy by Microbial Systems*

L. Packer, R.J. Mehlhorn, I.V. Fry, J.J. Maguire, S. Spath, G. Khomutov†, W. Nitchmann, E. Hrabeta-Robinson, M. Huflejt, J. Hrabeta, C. Reveron‡, J. Park, and K. Kondo

The Membrane Bioenergetics Group is investigating biological energy conversion mechanisms with reference to the roles played by membrane compartmentation, membrane structural components, and ion transport systems. Structure and function analyses are being integrated to present a complete picture of biological energy utilization. The use of salt (stress) is employed as a probe of bioenergetics in an obligate halophile (*Halobacterium halobium*) and in a fresh-water, halotolerant cyanobacterium (*Synechococcus* 6311).

H. Halobium

Intracellular pH was determined in cells loaded with the membrane-permeable precursor of the pH-sensitive fluorescent dye 2′, 7′-bis-(carboxyethyl)-5(6)-carboxyfluoresceinacetoxymethyl ester. The dye contains two carboxyl groups which are esterified with acetoxymethyl groups to yield an uncharged, membrane-permeable molecule. The permeable precursor is cleaved by cell esterases and the charged pH-sensitive dye remains trapped inside. This method proved to be a reliable indicator of internal pH and is currently being adapted to study the dynamic changes of cytosolic pH in response to changes in metabolism and environmental conditions in other bacteria.

Cyanobacteria

Magnetic resonance spectroscopy (electron paramagnetic and nuclear magnetic resonance) and gas chromatography have been used to determine the physical characteristics of the subcellular membrane systems with regard to viscosity, order parameter, and chemical composition. Major changes in viscosity and order parameter were observed in the cytoplasmic membranes but not in the thylakoid membranes under stress conditions. The lipid fraction exhibited modification in both membrane systems (an increase in the 18:1 fatty acid side chains). The data are consistent with an increase in the protein content of the cytoplasmic membrane. This finding is corroborated by increases in the number and size distribution of particles in the cytoplasmic membrane observed by freeze-fracture electron microscopy. We have developed several novel ESR and fluorescent methods that measure pH gradients inside cyanobacteria across both the cell and the thylakoid membranes. We have determined the effects of salt stress on intracellular pH and are developing a more detailed understanding of the ion channels in the cytoplasmic membrane. Our studies reveal that a major bioenergetic response which allowed cells to tolerate high salinity was a development of higher permeability to NaCl and increased respiration. Furthermore, from the response of internal volumes to various cations, the discovery of at least two different transport systems for Na^+ and NH_4^+ in control and salt-stressed cells can be deduced. One cation transport system is sensitive to amiloride, whereas the other is sensitive to L-methionine-D, L-sulfoximine. We have also developed an ESR method for measuring the concentration of oxygen inside living cells under conditions of active photosynthesis and respiration, and we have recently determined the highest concentration of oxygen observed so far in biological systems.

*This research was supported by the Office of Basic Energy Sciences of the U.S. Department of Energy under contracts DE-AC03-76SF00098 and DE-FG03-87ER13736 and NASA Interagency agreement A-14563c.

†A recipient of an IREX fellowship, under the US/Soviet exchange program.

‡LBL/JSU/AGMEF summer faculty program.

REFERENCES

1. Belkin S, Mehlhorn RJ, Hideg K, Hankovsky O, Packer L. Reduction and destruction rates of nitroxides. *Arch Biochem Biophys* 1987; *256*: 232-243.
2. Belkin S, Mehlhorn RJ, Packer, L. Determination of dissolved oxygen in photosynthetic systems by nitroxide spin-probe broadening. *Arch Biochem Biophys* 1987; *252*: 487-495.
3. Belkin S, Packer, L. Determination of dissolved oxygen in photosynthetic systems and protective strategies against its toxic effects in cyanobacteria. *In: Proceedings of the 2nd International Symposium held at Madurai,* on 11-14 December 1985. New Delhi: Today and Tomorrow's Printers and Publishers, 1987; 27-37.
4. Huflejt ME, Negulescu PA, Machen TE, Packer L. Na^+ and light-dependent regulation of cytoplasmic pH in cyanobacterium: *Synechococcus* 6311. *Biophys J* 1988; *53*: 616a.
5. Khomutov G, Packer L. Ion-binding properties of nonhomogenous biological membrane structure. (Submitted for publication, 1988)
6. Lefort-Tran M, Pouphile M, Spath S, Packer L. Cytoplasmic membrane changes during adaptation of the fresh water cyanobacterium *Synechococcus* 6311 to salinity. *Plant Phys J* 1988; *87*: 767-775.
7. McLaggen D, Belkin S, Packer L, Matin A. Electron spin resonance measurements of the effect of iono-

phores on the transmembrane pH gradient of an acidophillic bacterium. (Submitted for publication, 1988)
8. Nitschmann WH, Packer L. EPR studies on proton gradients and Na^+-NH_4^+ exchange during salt adaptation of Synechococcus 6311. *In: Proceedings of the 5th European Bioenergetics Conference, Aberystwyth,* 20-26 July 1988. (in press, 1988)
9. Packer L. The bioenergetics of stress responses in cyanobacteria. *In: Proceedings of Indo-US Workshop on Applications of Molecular Biology in Bioenergetics of Photosynthesis,* Delhi, India, 4-8 January 1988. (in press, 1988)
10. Packer L. Stress responses in cyanobacteria. *In: Receptors, Membrane Transport & Signal Transduction* [NATO ASI Series *Cell Biology*]. (in press, 1988)
11. Packer L, Hrabeta E, Robinson AE, Abdulaev NG, Kiselev AV, Taneva SG, Toth-Boconadi R, Keszthelyi L. Effect of cross linkers on the bacteriorhodopsin photocycle. *Biochem Biophys Res Comm* 1987; *145*: 1164-1170.
12. Packer L, Hrabeta-Robinson E, Stefka-Hristova G, Toth-Boconadi R, Keszthelyi L. Proton translocation by chemically modified bacteriorhodopsin. *Biochem In* 1987; *14*: 977-985.
13. Packer L, Spath S, Martin JB, Roby C, Blingy R. ^{23}Na and ^{31}P NMR studies of salt (NaCl) stressed fresh water cyanobacteria. *In: Proceedings of the 4th International Conference on Water and Ions in Biological Systems, Bucharest, Romania, 24-28 May 1987,* 1988; 335-346.
14. Tsujimoto K, Semadeni M, Huflejt M, Packer L. Intracellular pH of halobacteria can be determined by the fluorescent dye 2′,7′-bis(carboxyethyl)-5(6) carboxyfluorescein. *Biochem Biophys Res Comm* 1988; *88*: 123-129.

Detection and Prevention of Biological Free Radical Damage*

R.J. Mehlhorn, J.J. Maguire, K. Moore, B. Stone, J. O'Neil-Gonzalez, L. Packer and H. Rapoport

The study of oxidative free radical damage may prove to be the next major frontier of biological research, with profound implications for human welfare, including disease prevention and lifespan extension. The Membrane Bioenergetics Group has pioneered methods to detect free radicals and has applied these to both animal and plant systems.

*This work was supported by NIH (AG-04818) and LBL Director's funds for innovative research through the U.S. Department of Energy under contract DE-ACO3-76SF00098 and by the National Foundation for Cancer Research.

This project develops and applies ultrasensitive and non-destructive assays of oxidant stress in animals seeks to elucidate mechanisms of antioxidant action, including how vitamins C and E protect animals against free radicals. Our principal experimental approach is to use electron spin resonance (ESR), which detects magnetic moments associated with the unpaired electrons present in all free radicals. This basic approach is rendered highly sensitive by means of "free radical traps" that accumulate products of free radical reactions. We have developed such traps for detecting oxygen-, sulfur-, and carbon-centered free radicals, free transition metal ions, and non-radical oxidants that can be activated to form free radicals. In addition, we are developing a new chemical method whose basis is a radiolabeled chemical that can be injected into an animal, whereupon its reaction with hydroxyl and other strongly reactive oxyradicals causes the chemical to decompose into several fragments including a small, radiolabeled hydrocarbon fragment that will be volatilized in the lung and can be detected in expired breath.

Synthetic Work

We have implemented successful synthetic procedure for preparing the chemical free radical trap, alpha-keto-gamma-methylbutyric acid (KMBA), labeled so that ethylene derived from it contains a hydrogen isotope. The yields in this process are good, the compounds are stable and easily purified, and the hydrogen isotope is introduced via sodium borohydride. Since sodium borohydride of high specific activity is now available as a result of developments in the National Tritium Labeling Facility, we project liberated ethylene of specific activity ~25Ci/mmole from the labeled KMBA. We are studying release of ethylene from unlabeled and labeled KMBA, incorporation of tritium into KMBA, and development of more efficient analyses for the released ethylene.

Preparation of an ESR Probe of Transition Metal Ions and Buffer Purification Procedure

Treatment of the "stable" free radical 4-hydroxy-2,2,6,6-tetramethyl piperidine-N-oxyl (Tempol) with excess ascorbic acid reduced the nitroxide to its diamagnetic hydroxylamine, 4-hydroxy-2,2,6,6-tetramethyl piperidine-N-ol (designated as TOLH). TOLH undergoes only one-electron oxidation, making it suitable for free radical and transition metal ion detection. Initial experiments with TOLH revealed considerable variability of oxidation rates among different buffers, due to contamination with transition metal ions. An effective purification procedure was found to be treatment of the buffers with insoluble sodium phosphate glass, whose high negative charge density attracted the multivalent cations from the bulk aqueous phase, allowing them to be precipitated with the phosphate glass. Treatment of TOLH with cupric ions (cupric sulfate) catalyzed rapid oxidation to the nitroxide. Under aerobic conditions, this oxidation proceeded until all TOLH had become oxidized. Chelation of the copper with EDTA brought this oxidation to a virtually halt. Aqueous

ferric ion oxidized TOLH relatively slowly, but this rate was markedly accelerated by EDTA. Treatment with EDTA is thus a simple method for discriminating between copper and iron.

Detection of Thiyl Radicals with a Pyrroline Nitroxide

A Proxo nitroxide resistant to one-electron reduction by mild reducing agents like ascorbate was used to detect thiyl radicals. Glutathione was oxidized to thiyl radicals both chemically and enzymatically. The ESR signal of the nitroxide disappeared in buffered glutathione solutions aerobically but was quite stable under anaerobic conditions. Addition of traces of hydrogen peroxide to anaerobic glutathione caused rapid decreases in the nitroxide ESR signal, with more than three equivalents of nitroxide lost relative to the concentration of added peroxide. This non-enzymic reaction of nitroxides with glutathione was due to transition metal ions, since treatment with chelating agents inhibited the activity. A plausible mechanism of thiol activation is interaction of ferric ion with hydrogen peroxide to form the ferryl species, which abstracts a hydrogen atom from glutathione to form the glutathionyl radical. Glutathionyl also reacts with glutathione to form a species that reduces nitroxides to hydroxylamines. With horseradish peroxidase, phenol and hydrogen peroxide Proxo was both reduced and destroyed. Participation of thiyl radicals was confirmed by demonstrating that Proxo destruction was competitively inhibited by the spin trap DMPO, whose glutathionyl adduct was observed to increase to the same extent that Proxo destruction decreased.

The Production of Free Radicals by Thyroid Peroxidase

Peroxidase enzymes are well known to generate powerful oxidants in vitro. ESR measurements of TOLH oxidation have shown that can be used to accurately measure hydrogen peroxide, peroxidase activity, and phenol activity in tissue. We have applied TOLH to thyroid preparations from a variety of animals and demonstrated free radical production by peroxidase enzymes with an exogenous source of hydrogen peroxide and several phenols. We have thus established that enzymes present in animals can generate potent free radicals, provided that sufficient hydrogen peroxide and phenolic equivalents are present.

Bilayer Permeability of Liposomes to Methyl Radicals

A flavin-based photochemical system for generating methyl radicals outside asolectin liposomes was used to demonstrate that these radicals readily cross bilayer membranes. The liposomes were prepared such that an impermeable nitroxide was trapped inside them. Photochemical generation of methyl radicals outside the liposomes destroyed both internal and external populations of the nitroxide (as seen in the decay of their ESR signals), demonstrating that lipid bilayers are not effective barriers to the movement of alkyl radicals. This is important for understanding free radical mutagenesis and carcinogenesis because it demonstrates that lipid peroxidation products from metabolically active membranes like mitochondria can migrate across the nuclear membrane to interact with DNA.

Studies of One-Electron Tocopherol Oxidation and Reduction

The tocopheroxyl radical was observed by ESR in liposomes containing physiologic concentrations of alpha-tocopherol. The one-electron oxidation of tocopherol was catalyzed by horseradish peroxidase and the hydrophilic phenol arbutin with either direct addition of hydrogen peroxide or with a glucose oxidase system. In di-oleyl phosphatidyl choline liposomes, the tocopheroxyl radical could be observed for several hours with the glucose oxidase system and, after an initial decay period, a residual fraction of the alpha tocopherol was also stable. These results indicate that under appropriate conditions in biomembranes, the tocopheroxyl radical can be stable and that radical dimerization is not a facile pathway for its destruction. We also applied this enzymic oxidizing system to liver microsomes and submitochondrial membranes and showed that the tocopheroxyl radical could be produced in sufficient concentrations to be ESR-detectable in membranes isolated from rats that had been fed vitamin E-enriched diets. The radical in the subcellular membranes was also stable in the presence of the enzymic generating system but decayed rapidly when enzyme activity was arrested by removing oxygen.

Impacts and Multiple Iridium Anomalies*

F. Asaro, H.V. Michel, L.W. Alvarez‡, W. Alvarez†, and A. Montanari†

A geochemical study has been made of nearly 60 meters of limestone deposited during a period of 5 million years near the Cretaceous-Tertiary (K-T) boundary in the Bottaccione Gorge near Gubbio, Italy. Except in 2.6 meters of rock directly adjacent to the huge K-T iridium (Ir) spike, no Ir anomalies were observed, and the average Ir background was 12.6 x 10^{-12} gram of Ir per gram of rock (ppt). Close to the spike, however, are about a dozen Ir peaks ranging from 20 to 80 ppt above background.

In a study with H.R. Bowman, we observed that the Ir peaks in the Tertiary disappeared when ratios were taken to abundances of elements in clay, e.g., Fe, Si, and Al. The continuous and nearly exponential nature of the resulting curves suggests that the deposition of Ir was not episodic, and so the Ir is not due to volcanism or impacts of comet clusters. Washing of the continents following the K-T impact is a possible Ir source.

The Cretaceous Ir peaks, on the other hand, do not disappear when ratios are taken to the abundance of clay elements, and they may be due to diffusion.

Multiple Ir anomalies have been detected in Late Eocene deposits (impact-related) and (with Erle G. Kauffman) at the Cenomanian-Turonian boundary (probably mantle-related).

A single Ir peak in 11.7-million-year-old sediment has been observed (with Mark H. Anders) in one location (DSDP hole 588B) in a study of a continuous 53-meter section.

*This work was supported by the Director, Office of Energy Research, Office of Basic Energy Sciences, Chemical Sciences Division, of the U.S. Department of Energy under Contract No. DE-ACO3-76SF00098.

†Department of Geology & Geophysics, University of California, Berkeley, CA 94720

‡Emeritus Professor of Physics, University of California, Berkeley. Professor Alvarez died September 1, 1988.

A Study of the Relation Between Volcanism in the Weddell Sea about 65 Million Years Ago and the Cretaceous-Tertiary Bolide Impact*

H.V. Michel, F. Asaro, W. Alvarez†, and L.W. Alvarez‡

In a study of cores from ODP Hole 689B, no iridium (Ir) anomaly was found in sections 1 through 6 of core 25 or in core 26 from the top down to section 2, 3-12 cm. The background in clay-poor sediments averaged 11 parts-per-trillion (ppt) Ir, and a clay-enriched region had nearly the same average, 26 ± 12 ppt. If the Cretaceous-Tertiary (K-T) contact is in the region studied, then the K-T boundary was probably either not deposited or it was eroded away.

In a study of cores 15 and 16 of ODP Hole 690C, an iridium peak of 1566 ± 222 ppt was found in section 4 of core 15, 39-40 cm with a half width of 6.6 cm. Background abundances were ~15 ppt, and distinctly higher Ir abundances were observed from 119 cm below to 71 cm above the main peak. The Ir abundances were measured with the Iridium Coincidence Spectrometer (ICS) following neutron activation. The abundances of many other elements were measured by conventional techniques of gamma ray spectrometry after neutron irradiation. Iron abundance data and ratios of the abundances of Ir, Sc, Cs and Co to those of iron are shown (Figure).

The main Ir peak occurs where the fossil forms change from Cretaceous to Tertiary, and this peak has been shown to be due to an impact on the Earth of an asteroid or comet about 10 km in diameter. The Ir distribution below the main peak is attributed to bioturbation by organisms with burrows extending at least 0.4 meter.

*This work was supported by the Director, Office of Energy Research, Office of Basic Energy Sciences, Chemical Sciences Division, of the U.S. Department of Energy under Contract No. DE-ACO3-76SF00098.

†Department of Geology & Geophysics, University of California, Berkeley, CA 94720.

‡Emeritus, Professor of Physics, University of California, Berkeley. Professor Alvarez died September 1, 1988.

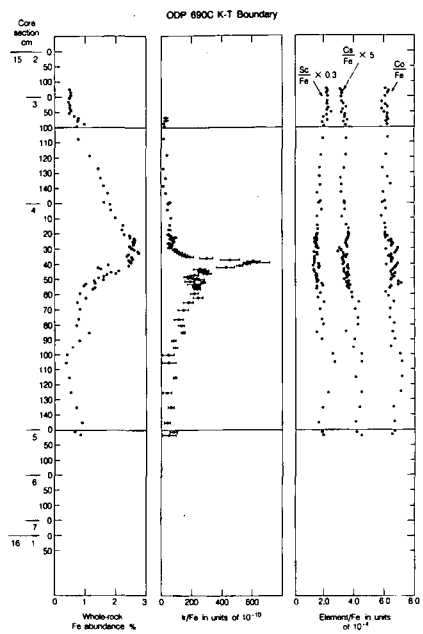

Figure. Ocean Drilling Program Leg 113 Hole 690C K-T Boundary. (XBL 889-8541)

The Ir distribution above the main peak may have the same cause, but other explanations may be significant.

In this work, we wished to determine whether volcanism in this region might have been triggered by the K-T impact. Clay, an alteration product of volcanic glass, is sometimes taken as an indication of volcanism.

The mainly $CaCO_3$ sediment of core 15 contains variable enrichments of clay, and the onset of the most intense deposit is found (within 2 cm) in the same position as the main Ir peak. The clay deposit, estimated to be about 50% of the sediment, extends upward ~19 cm and then slowly decreases to a background level of 10% over 1 meter. The degree of homogeneity of the clay deposit suggests it was not caused by episodic volcanism but may have been caused by a decreased $CaCO_3$ deposition rate possibly triggered by the K-T impact.

Sources of Quartzite in Ancient Egyptian Sculptures*

F.H. Stross, R.L. Hay†, F. Asaro, H.R. Bowman, and H.V. Michel

Despite its great hardness and toughness, which makes it difficult to work, quartzite was used frequently in ancient Egypt in sculptures and architecture. Several quartzite deposits are known in Egypt, but the artifacts studied at the Lawrence Berkeley Laboratory appear to have derived from only two major deposits: Gebel el Ahmar (located near Cairo) and an area encompassing three contiguous quarries opposite and just north of Aswan. The LBL studies were made on the Colossi of Memnon in the Plain of Thebes and on a number of quartzite deposits known to have been (or which could have been) worked. The Gebel el Ahmar and Aswan quarry samples could be readily distinguished from other quarry samples by low abundances of calcium, manganese, and sodium.

The Gebel el Ahmar quarry is located about 680 km north and downstream from the Plain of Thebes, where the Colossi repose; the Aswan quarries are about 210-220 km south of Thebes. In our previous work, we found that the Colossi originally were made from rock taken from the Gebel el Ahmar quarry, whereas the blocks used by the Romans 1600 years later for large-scale reconstruction of the northern Colossus came from the Aswan deposit.

Knowing that the quartzite originally used for the Colossi came from the Cairo quarry, we are interested in discovering the sources of other artifacts of that era. In earlier work during the first field trip, a number of samples were collected from sculptures other than the Colossi. These and additional samples came from artifacts originally located at Thebes and its vicinity and also near Cairo; the samples include carvings from the reigns of kings of the New Kingdom (sixteenth to eleventh centuries B.C.).

The specimens under study were subjected to neutron activation analysis (NAA). Some of the specimens were

*This work was supported by the Director, Office of Energy Research, Office of Basic Energy Sciences, Chemical Sciences Division, of the U.S. Department of Energy under Contract No. DE-AC03-76SF00098.

†Department of Geology, University of Illinois, Urbana, IL 61801.

also subjected to petrographic studies. Results of the NAA and petrographic studies, with the possible exception of samples with ambiguous or questionable provenience show that stela (or false door of Tutankhamen) in Thebes is the only object in the suite that appears to have used Aswan rather than Gebel el Ahmar quartzite. It would have been made little more than two decades after the death of Amenhotep III and would be the first quartzite carving shown to have used Aswan quartzite in pharaonic times. Later use is demonstrated by the unfinished obelisk of Seti I, still located in the Aswan quarries and which would have been carved about half a century after the reign of Tutankhamen.

REFERENCE

1. Stross FH, Hay RL, Asaro F, Bowman HR, and Michel, HV. Sources of the Quartzite of some Ancient Egyptian Sculptures. *Archaeometry* 1988; 30(Pt 1): 109-119.

Possible Worldwide Middle Miocene Iridium Anomaly and its Relation to Periodicity of Impacts and Extinctions*

F. Asaro, W. Alvarez†, H.V. Michel, L.W. Alvarez§, M.H. Anders†, A. Montanari†, and J.P. Kennett‡

In a study of one million years of Middle Miocene sediment deposition in ODP Hole 689B in the Weddell Sea near Antarctica, a single iridium (Ir) anomaly of (44 ± 10) x 10^{-12} gram Ir per gram rock (ppt) has been observed in core 6H, section 3, 50-60 cm, after background contributions associated with manganese precipitates and clay are subtracted. ODP Hole 689B is 10,000 km away from another site (DSDP Hole 588B in the Tasman Sea north of New Zealand), where a single Ir anomaly of 144 ± 7 ppt over a background of 11 ppt (core 25, section 2, 20-30 cm) was found in an earlier study of 3 million years of deposition. From chemical measurements the latter deposition was thought to be impact-related. Ir measurements were made with the Iridium Coincidence Spectrometer after neutron activation.

The age-versus-depth calibration curves given in the DSDP and ODP preliminary reports indicate the ages of the Ir anomalies are identical (11.7 million years), but the absolute and relative uncertainties in the curves are not known. Based on the newest age data, the age estimate is 10 million years.

Because the Ir was deposited at the two sites at about the same time (within our ability to measure) and the sites are one quarter of the way around the world from each other, the deposition seems likely to have been worldwide. The impact of a large asteroid or comet could produce the wide distribution, and the data support of impact relationship deduced for DSDP 588B from the chemical evidence. If the surface densities of Ir at the two sites represent the worldwide average, the diameter of a C1-type asteroid containing the necessary Ir would be 3 ± 1 km, large enough to cause worldwide darkness, and hence extinctions. This would be the third worldwide stratigraphic horizon of impact-related Ir-enriched rocks found, their ages being 65-66.7 (K-T boundary), 37-39.4 (Late Eocene), and 10-11.7 (Middle Miocene) million years. This spacing suggests a periodicity of 27-28 million years for the impact of large extraterrestrial bodies in agreement with those reported for extinctions and crater ages although both of the latter have been disputed.

Another stratigraphic horizon of Ir-enriched rocks has been observed in rocks about 91-92 million years old from North America, Italy, and Poland. Some of the rocks have a mantle signature, but the possibility of an impact on the ocean bottom cannot be ruled out as the source of the anomaly. An impact-related horizon has been observed in 2.3-million-year-old rocks distributed over 600 km. The minimum size of the bolide was reported as 0.5 km, which may be borderline for producing worldwide darkness. Anomalous Ir abundances have been observed at the Callovian-Oxfordian boundary in Spain and Poland. The origin of the Ir has not yet been well determined, and the chronological age is uncertain by many millions of years. Precambrian impact-related Ir deposits have been found in rocks about 3.5 billion years old in South Africa and possibly Australia; these rocks are too old to check the correlation with the observed periodicity.

*This work was supported by the Director, Office of Energy Research, Office of Basic Energy Sciences, Chemical Sciences Division, of the U.S. Department of Energy under Contract No. DE-AC03-76SF00098.

†Department of Geology and Geophysics, University of California, Berkeley, CA 94720.

‡Department of Geological Sciences, University of California, Santa Barbara, CA 93106.

§Emeritus Professor of Physics, University of California, Berkeley. Professor Alvarez died September 1, 1988.

LAWRENCE BERKELEY LABORATORY
TECHNICAL INFORMATION DEPARTMENT
1 CYCLOTRON ROAD
BERKELEY, CALIFORNIA 94720